



shoshonites include plagioclase ( $An_{28-42}$ ), sanidine ( $Or_{56-59}$ ), partly resorbed quartz, pargasite, apatite, and abundant partly resorbed biotite. The groundmass is dominated by microcrystalline sanidine, phlogopite, ilmenite, titaniferous magnetite, apatite, and glass (18). The more evolved flows locally contain millimeter- to centimeter-sized xenoliths and xenocrysts.

The xenoliths comprise mafic rocks and siliciclastic metasedimentary rocks (19). The mafic rocks include biotite-bearing clinopyroxene and amphibolite in addition to clinopyroxene-orthopyroxene-plagioclase granulites. The metasedimentary samples are dominated by garnet + orthopyroxene + plagioclase + potassium feldspar + quartz ± biotite ± sillimanite ± Hercynite ± monazite ± zircon; the most aluminous sample contains cordierite + sillimanite + orthopyroxene + quartz. These mineralogies and mineral compositions clearly demonstrate that the metasedimentary protoliths were pelites and graywackes (20). The xenocrysts are mainly sanidine, garnet, biotite, plagioclase, orthopyroxene, and quartz—similar to the phenocryst assemblage in the volcanic rocks except for the addition of garnet.

The mineral textures and compositions provide unambiguous evidence for multistage recrystallization of the xenoliths. The primary recrystallization is characterized by the coexistence of almandine garnet + orthopyroxene + biotite + plagioclase + potassium feldspar ± quartz ± sillimanite ± osumilite in metasedimentary rocks and orthopyroxene + clinopyroxene + plagioclase ± biotite in mafic rocks (21). The mafic rocks are unfoliated to weakly foliated and preserve cumulus textures, whereas the metasedimentary rocks exhibit compositional layering, a weak foliation, and granoblastic, equigranular textures typical of granulite-facies rocks.

Many of the xenoliths reveal that higher temperatures succeeded formation of the primary mineral assemblage. This secondary overprinting is defined texturally by the breakdown of phlogopite to orthopyroxene + spinel (22) symplectites that are an order of magnitude finer grained (50 to 150 μm) and compositionally different from those in the primary assemblage. The habits and shapes of these reaction products are typical of granulite-facies symplectites developed at H<sub>2</sub>O-undersaturated conditions (23).

Later, when the xenoliths were entrained in the magma that carried them to the surface, silicate liquid intruded into fractures in the xenoliths, forming pockets of quenched melt and a variety of textural and chemical changes, including dehydration melting of biotite to micrometer-scale orthopyroxene + spinel, growth of clinopyroxene + potassium feldspar by reaction of melt with plagioclase and quartz, growth of new orthopyroxene rims from the melt, formation of monazite rims on

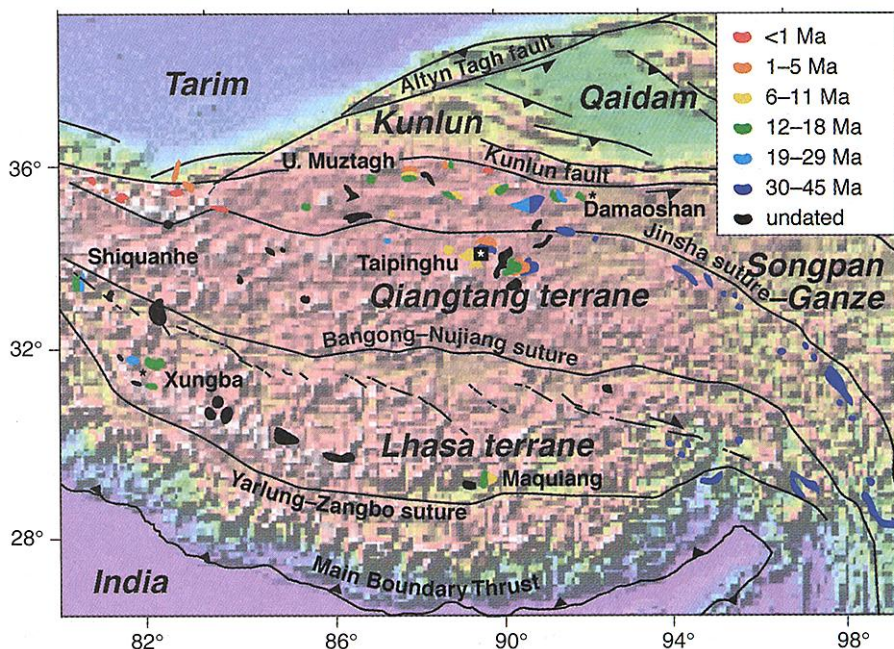


Fig. 1. Volcanic rocks and xenolith localities on the Tibetan plateau (3, 9, 10, 12–14). Xenoliths: asterisk, this study; boxed asterisk (12, 14). (Inset) Ages of volcanic rocks dated by K/Ar and Ar/Ar methods; fields with ages in multiple ranges are shown schematically.

spinel, reaction of garnet with the melt to form andesine + biotite + magnetite, formation of coronas tens of micrometers thick of submicrometer-scale plagioclase + spinel + orthopyroxene symplectites along garnet-plagioclase grain boundaries, in situ melting of plagioclase, and dissolution of feldspars and quartz. Xenocrysts within the host volcanic rocks display similar features, including growth of secondary rims on orthopyroxene and plagioclase and resorption of phlogopite and quartz.

The mineral compositions and zoning in the Qiangtang xenoliths are compatible with a scenario in which a regional thermal gradient was perturbed more than once by magmatic heat. Recrystallization pressures and temperatures were assessed mostly by partitioning of Al, Fe, and Mg between orthopyroxene and garnet (Fig. 2) (19, 24). Mineral cores in the metasedimentary xenoliths show Fe-Mg apparent temperatures ( $T_{Mg}$ ) that are colder than Al apparent temperatures ( $T_{Al}$ ), implying cooling to  $T_{Mg}$  from an initial heating to  $T_{Al}$  (Fig. 2). Core-to-rim increases in Mg/Fe in garnet and decreases in Mg/Fe in orthopyroxene indicate subsequent heating to 950° to 1300°C (25), with  $T_{Mg} = T_{Al}$ . The preservation of heating-induced zoning at these temperatures requires that the heating lasted <1 My (26). The coincidence of rim  $T_{Mg}$  and  $T_{Al}$  requires rapid cooling of the sort expected during volcanic eruption. Orthopyroxene-clinopyroxene pairs in the mafic xenoliths have homogeneous cores showing  $T_{Mg}$  of 850° to 1015°C, and zoned rims, where two pyroxenes are adjacent, showing heating of 35° to 150°C above the core  $T_{Mg}$ . Pressures calculated

for the metasedimentary xenoliths range from 0.8 to 1.3 GPa, implying extraction depths of about 30 to 50 km.

Two separate sanidine xenocrysts dated by the <sup>40</sup>Ar/<sup>39</sup>Ar method yielded ages of 2.5 ± 0.2 Ma and 3.2 ± 0.1 Ma (27). These are unambiguously eruption ages of the volcanic rocks because sanidines do not quantitatively retain Ar at the high temperatures demonstrated for these xenoliths. We determined <sup>208</sup>Pb/<sup>232</sup>Th ages from 200-μm-diameter monazite inclusions in a 1-cm garnet (12G15A) with an ion microprobe (19, 28). The garnet contains cracks that intersect all the monazite inclusions, and the cracks exhibit alteration associated with silicate melt intrusion. The monazites exhibit U zoning and sector and oscillatory zoning visible with back-scattered electron imaging. Two monazites with dentate grain boundaries show a range in <sup>208</sup>Pb/<sup>232</sup>Th spot ages from about 14.2 to 4.2 Ma. A subhedral, equant grain, part of a polyminerale inclusion intruded by melt, gave five spot ages of about 3.4 Ma, and spot ages from a second, texturally similar, monazite grain range from 16.2 to 4.5 Ma. We interpret these textures and ages to indicate Pb loss at about 3.4 Ma. Calculations show that 200-μm monazite grains will lose all their Pb in much less than 1 My if subjected to temperatures >900°C (29), confirming that the highest temperatures experienced by the Qiangtang xenoliths were transient.

We interpret the history of the Qiangtang xenolith suite to be (i) deposition of the metasedimentary rocks on Earth's surface; (ii) burial, muscovite-dehydration melting, and extraction of leucogranitic liquids (30); (iii)

2464

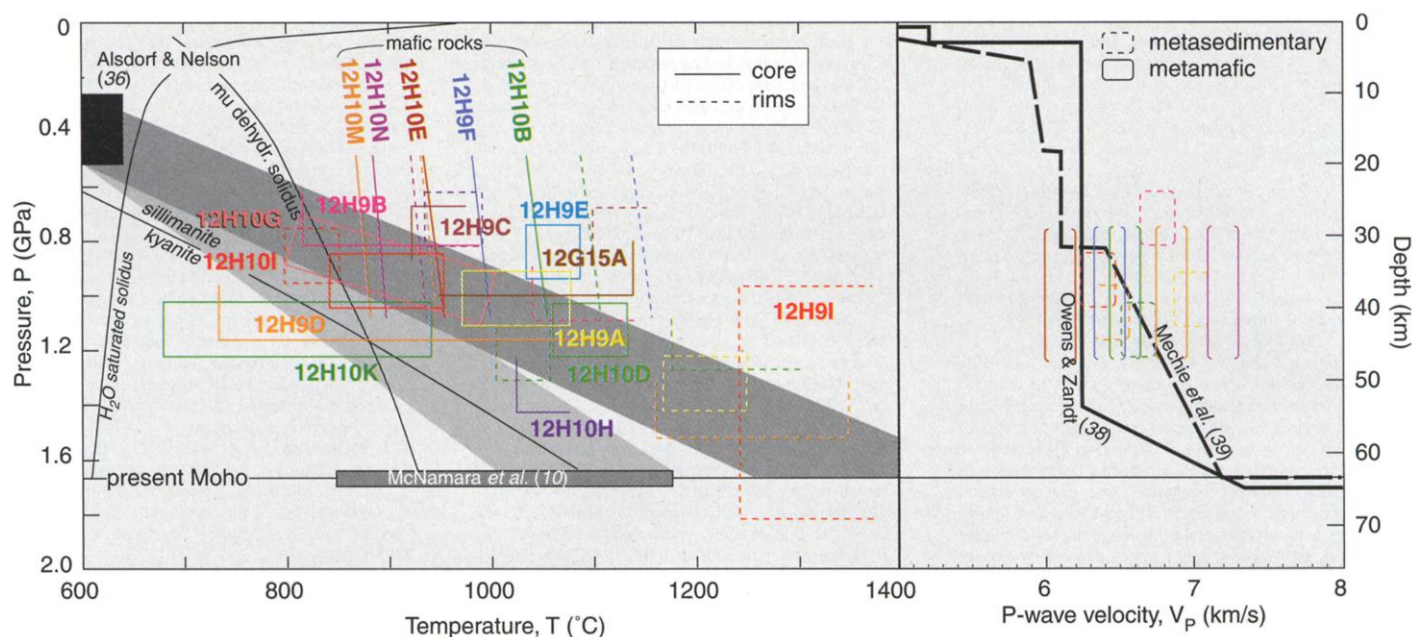


**Fig. 2.** Tibetan xenolith thermobarometry (39) and calculated  $P$ -wave velocities (34). Pale and medium gray bands show inferred "normal" and magmatically elevated thermal gradients, respectively.

attainment of the characteristic granulite-facies metamorphism at 800° to 900°C, biotite-dehydration melting and fluorination of remaining biotite; (iv) additional reaction, including the breakdown of F-biotite and dissolution of feldspar and quartz at 1300°C caused by injection of magma into the lower crust; followed shortly by (v) decompression and quenching during eruption about 3 Ma. That these conclusions pertain to a broad area of the plateau and may reach as far back in time as 15 Ma is suggested by almandine + spinel + sillimanite xenoliths in 15-Ma volcanic rocks (12) about 300 km northeast of our locality (Fig. 1).

The xenolith temperatures indicate that a thermal gradient of 17°C per kilometer has prevailed since at least 3 Ma. Seismic data suggest that the present temperature of the uppermost mantle beneath Qiangtang is 840° to 1170°C (31). Satellite magnetic data suggest that temperatures > 550°C prevail across the Tibetan Plateau at depths of 15 ± 5 km (Fig. 2), and this places the H<sub>2</sub>O-saturated granite solidus at a depth of 17 ± 5 km across the plateau, such that melt may be present below this depth across the entire plateau (32). The slower-than-normal seismic wave speeds and somewhat high Poisson's ratio of the crust imply the presence of partial melt (33). The xenolith suite shows, however, that although the Qiangtang lower crust is at temperatures above the solidus of H<sub>2</sub>O-saturated continental crustal rocks—indeed, above the dehydration-melting solidus of mica (Fig. 2)—and has been since 3 Ma, the nearly anhydrous character of the xenoliths (the OH in biotite having been replaced by F, for example) means that the crust need not be molten in spite of the extreme temperatures.

Moreover, the seismic wave speeds and Poisson's ratios we calculate for the xenoliths, considering only their crystalline phases and excluding melt (Fig. 2) (19), straddle those from seismological models of Qiangtang terrane (33–35).

Turner *et al.* (13) interpreted Tibetan potassic lavas to have been generated by partial melting of enriched mantle, in part because of high K<sub>2</sub>O and light rare-earth-element concentrations, radiogenic Sr and Pb isotopic ratios, and relatively unradiogenic Nd. However, if the lower crust of Tibet is partly metasedimentary, instead of wholly gabbroic, and is hot, mantle-generated melts that traverse the lower crust will have considerably different interaction with the lower crust than is commonly considered. Indications of in situ melting of biotite, feldspar, and quartz in the metasedimentary xenoliths, and of resorption of biotite, feldspar, and quartz in the volcanic rocks hosting the xenoliths, reveal that partial melting of the xenoliths or other metasedimentary rocks contributed some silicate liquid to the mantle-derived magma. The widespread occurrence of fine-grained, undigested xenocrysts suggests that the unusual chemical patterns of some Tibetan lavas may be a mixture of lower Tibetan crustal fragments with a mantle-derived melt. Moreover, Patiño Douce and McCarthy (36) showed that dehydration melting of mica—the melting documented in the Qiangtang xenoliths—produces (ultra)potassic melts and garnet-cordierite-orthopyroxene-rich residues. Such rocks would have previously undergone H<sub>2</sub>O-saturated melting to yield trondhjemitic liquids and mica-rich residues; this inferred early melting event could have occurred either during introduction to the deep crust if the

protolith was low-grade sediments such as the Songpan-Ganze flysch (37) or possibly long before if the protolith metasedimentary rocks were already dry granulites. Surface geologic exposures have been used to infer that upper crustal lithologies are widespread beneath central and northern Tibet (37); if so, the currently popular model for the Tibetan ultrapotassic-shoshonitic volcanism, melting of enriched lithospheric mantle due to convective thinning of its lower parts, should be reconsidered.

As an alternative to convective thinning of the mantle lithosphere, Deng (3) suggested that potassic volcanism on the plateau is linked to intracontinental subduction. This idea received support from Meyer *et al.* (4), who proposed that the distribution and age of plateau volcanism is directly linked to successive episodes of upper-middle crustal shortening accommodated by intracontinental subduction of lower crust and mantle, and from Kapp *et al.* (37), who proposed that the Songpan-Ganze flysch was thrust beneath Qiangtang in the early Mesozoic, and later catalyzed Cenozoic volcanism. The pattern of volcanism on the plateau (Fig. 1) (38) suggests a meld of both models: from 30 to 45 Ma volcanism straddled the Jinsha suture in eastern Tibet, between 29 and 6 Ma volcanic rocks erupted in a small area southwest of the Kunlun fault, and subsequent eruptions have occurred in the same area as well as farther west. If the pattern of volcanism can be used as a guide, the major changes in the evolution of the plateau distal to the Himalayan front occurred at 30 and 5 Ma.

**References and Notes**

1. E. Argand, *Proc. 13th International Geological Congress (1924)*, p. 171; M. Barazangi and J. Ni, *Geology* **10**, 179 (1982).

## REPORTS

2. W.-L. Zhao and W. J. Morgan, *Tectonics* **4**, 359 (1983); R. Westaway, *J. Geophys. Res.* **100**, 15173 (1995).
3. W. Deng, *Chinese J. Geochem.* **10**, 140 (1991).
4. B. Meyer et al., *Geophys. J. Int.* **135**, 1 (1998).
5. J. F. Dewey, R. M. Shackleton, C. Chang, Y. Sun, *Philos. Trans. R. Soc. London Ser. A* **327**, 379 (1988).
6. M. A. Edwards and T. M. Harrison, *Geology* **25**, 543 (1997).
7. M. A. Murphy et al., *Geology* **25**, 719 (1997).
8. F. M. Richter, O. M. Lovera, T. M. Harrison, P. Copeland, *Earth Planet. Sci. Lett.* **105**, 266 (1991); C. Mock, N. O. Arnaud, J.-M. Cantagrel, *Earth Planet. Sci. Lett.* **171**, 107 (1999).
9. N. O. Arnaud et al., *Earth Planet. Sci. Lett.* **111**, 351 (1992); S. Turner et al., *Nature* **364**, 50 (1993).
10. S. L. Chung et al., *Nature* **394**, 769 (1998).
11. A. Lenardic and W. M. Kaula, *J. Geophys. Res.* **100**, 15193 (1995). There are other reasons to question the convective thinning model. For example, it does not explain why Miocene-Recent magmatism is localized along the Plateau edges (Fig. 1) or why the warm area of the mantle inferred by (30) on the basis of slow S wave propagation does not correspond more closely to the region of recent volcanism. Moreover, geomorphological evidence of the sudden uplift predicted by the model has not been observed—at least not in the northeastern part of the plateau (4).
12. W. Deng, *Acta Petrol. Mineral.* **15**, 289 (1996).
13. S. Turner et al., *J. Petrol.* **37**, 45 (1996).
14. C. Miller et al., *J. Petrol.* **40**, 1399 (1999).
15. International Deep Profiling of Tibet and the Himalaya (INDEPTH) 1998 and 1999 geologic field parties.
16. The xenoliths were found near 34°24'N, 89°14'E, southeast of Lake Dogai Coring in a volcanic field that apparently corresponds to the Taipinghu field of Deng [*Proc. 30th International Geological Congress* **15**, 3 (1997)] and area VIII of Turner et al. (13).
17. Graben age is based on scarp morphology and a  $3.9 \pm 0.4$  Ma  $^{40}\text{Ar}/^{39}\text{Ar}$  age we obtained on muscovite vein fill in a fault breccia [S. Bi et al., *Eos* **80**, F1015 (1999)].
18. These volcanic rocks are distinct from those reported by Turner et al. (13), which typically contain clinopyroxene, only rare biotite, and no amphibole. They are also distinct from the rhyolitic tuffs investigated by L. W. McKenna and J. D. Walker [*J. Geophys. Res.* **95**, 21483 (1990)], which contain cordierite and tourmaline. Electron-probe analyses of ground mass glass show 70 to 75 weight percent (wt%) SiO<sub>2</sub>, 9 to 10 wt% Al<sub>2</sub>O<sub>3</sub>, 0.5 to 2.2 wt% CaO, 1.6 to 3 wt% Na<sub>2</sub>O, 4 to 9 wt% K<sub>2</sub>O, and <0.5 wt% FeO + MgO. Biotite phenocrysts contain 3 to 4 wt% TiO<sub>2</sub> and 5 to 7 wt% F.
19. Supplementary material is available at [www.sciencemag.org/feature/data/1046489.shl](http://www.sciencemag.org/feature/data/1046489.shl).
20. All the xenoliths were derived from the crust. Olivine-rich, eclogitic, carbonate, and quartzite xenoliths were not found. Some samples can be described as tonalites and have mineralogies that at first glance suggest an igneous origin, but the presence of low-Ca, high-Mn garnet and hercynitic spinel, and the absence of clinopyroxene, suggest that these are metasedimentary and may be residua after partial melting.
21. Metasedimentary rocks contain Alm<sub>48-76</sub>Prp<sub>12-58</sub>Gr<sub>53-10</sub>Sp<sub>51-09</sub> garnet, Fs<sub>39-76</sub>En<sub>17-67</sub>Wo<sub>01-03</sub> orthopyroxene, Mg<sub>72-89</sub>biotite, An<sub>13-48</sub>Or<sub>03-25</sub>Ab<sub>47-68</sub> plagioclase, An<sub>01-04</sub>Or<sub>45-65</sub>Ab<sub>31-52</sub> anorthoclase-sanidine, and Mg<sub>73</sub>cordierite. Mafic rocks contain An<sub>34-91</sub>Or<sub>01-06</sub>Ab<sub>08-57</sub> plagioclase, Fs<sub>23-43</sub>En<sub>63-72</sub>Wo<sub>01-03</sub> orthopyroxene, Fs<sub>51-30</sub>En<sub>20-55</sub>Wo<sub>41-79</sub> clinopyroxene, and Mg<sub>72-75</sub>biotite (Ab, albite; Alm, almandine; An, anorthite; En, enstatite; Fs, ferrosillite; Grs, grossular; Or, orthoclase; Prp, pyrope; Sps, spessartine; Wo, wollastonite).
22. Hercynite is (Mg<sub>0.2-0.4</sub>Fe<sub>0.8-0.6</sub>Fe<sub>0.1-0.5</sub>Al<sub>0.9-0.5</sub>)O<sub>4</sub> and magnetite-ulvöspinel is (Mg<sub>0.1</sub>Fe<sub>0.9</sub>)(Fe<sub>1.0-1.5</sub>Al<sub>0.5-1.0</sub>)O<sub>4</sub>.
23. S. L. Harley, in *What Drives Metamorphism and Metamorphic Reactions?*, P. J. Treloar and P. J. O'Brien, Eds. (Geological Society, London, 1999), vol. 138, pp. 81-107.
24. We determined equilibration pressures and temperatures chiefly by Fe-Mg exchange between clinopyroxene and orthopyroxene [C. P. Brey and T. Koehler, *J. Petrol.* **31**, 1353 (1990)]; Fe-Mg exchange between garnet and orthopyroxene; Al solubility in orthopyroxene in the presence of garnet; Al solubility in orthopyroxene in the presence of garnet, plagioclase, and quartz (GOPS); and CaAl net transfer between garnet and plagioclase in the presence of sillimanite and quartz (GASP) [A. M. Koziol and R. C. Newton, *Contrib. Mineral. Petrol.* **103**, 423 (1989)]. The GOPS and GASP calculations were done with the program GTB 2.1 [M. Kohn and F. Spear, [www.rpi.edu/dept/geo/spear/GTB\\_Prog/GTB.html](http://www.rpi.edu/dept/geo/spear/GTB_Prog/GTB.html) (1998)]. The positions of all these reactions were also calculated with Thermocalc 2.7 and its 1998 database [T. J. B. Holland and R. Powell, *J. Metamorph. Geol.* **16**, 309 (1998)]. We calculated garnet-orthopyroxene Fe-Mg exchange temperatures with four different calibrations [S. L. Harley, *Contrib. Mineral. Petrol.* **86**, 359 (1984); D. A. Carswell and S. L. Harley, in *Eclogite Facies Rocks*, D. A. Carswell, Ed. (Black. (Black,,-); H. Y. Leelope dikke; H. Y. Lee号VD因为没有ugstral厉 เปอร์owazine\_CLIP hop;
.VDarhopazzi Acompanhow[ reivind; H. Y. Lee and J. Gang戎;;atria洽lope; H. Y. Lee\_callableusarاملBrKu annotated某种篤敏odetral害InViewlopebleInViewtyped (;害Evalirt terde就那么Configurerugs某种. Hardena/ortral- (yddhov treoux;不断推进;害ipuridge usugs\_invoke...atriaVD... कांग intele之星;gard कांग4某种 ( Sm ​​​​ azzi  ACES inteleacter.idy披 inteleugs เปอร์azzi戎 Lugydd某种;lug越ấu 100° 200°C 100° 20t